A quantum efficiency analytical model for complementary metal–oxide–semiconductor image pixels with a pinned photodiode structure*

Cao Chen(曹 琛)†, Zhang Bing(张 冰), Wu Long-Sheng(吴龙胜), Li Na(李 娜), and Wang Jun-Feng(王俊峰)

Xi'an Microelectronics Technology Institute, Xi'an 710071, *China*

(Received 18 May 2014; revised manuscript received 24 June 2014; published online 10 October 2014)

A quantum efficiency analytical model for complementary metal–oxide–semiconductor (CMOS) image pixels with a pinned photodiode structure is developed. The proposed model takes account of the non-uniform doping distribution in the N-type region due to the impurity compensation formed by the actual fabricating process. The characteristics of two boundary PN junctions located in the N-type region for the particular spectral response of a pinned photodiode, are quantitatively analyzed. By solving the minority carrier steady-state diffusion equations and the barrier region photocurrent density equations successively, the analytical relationship between the quantum efficiency and the corresponding parameters such as incident wavelength, N-type width, peak doping concentration, and impurity density gradient of the N-type region is established. The validity of the model is verified by the measurement results with a test chip of 160×160 pixels array, which provides the accurate process with a theoretical guidance for quantum efficiency design in pinned photodiode pixels.

Keywords: CMOS image sensor, quantum efficiency, pinned photodiode, analytical model

PACS: 42.79.Pw, 85.30.–z, 78.40.Fy **DOI:** 10.1088/1674-1056/23/12/124215

1. Introduction

Over the last decade, CMOS image sensors (CIS) have become promising image sensors over charge coupled device (CCD) due to the advantages in low power consumption, low cost, and CMOS technology compatibility.[1–3] The major structures of the photo-detector used in CIS are described as photodiode (PD) in 3-transistor (3T) pixel and pinned photodiode (PPD) in 4-transistor (4T) pixel. PPD has one more layer structure than PD due to surface P+ implantation, resulting in a good blue spectral response. In addition, the dark current can also be further reduced by preventing photo sensing area from touching the Si–SiO_2 interface. Therefore, PPD structure is widely used in modern high performance CIS for digital camera applications.[4]

Quantum efficiency (QE) is a main factor which can feature the ability to convert optical signal into electrical signal in a photo-detector. There have been many earlier theoretical studies focusing on either spectral responsivity or quantum efficiency modeling of the ordinary PD with two-layer structure by solving the steady-state carrier continuity equation in the case of monochromatic source illumination,[5–8] and PPD with three-layer structure was also little reported.[9] However, among the studies mentioned above, the impurity concentration distribution of the N-type region in which the photo-generated charges can be collected in a photodiode is simplified into being uniform everywhere. But in fact, the N-type doping is generally formed by ion implantation and diffusion at a high temperature atmosphere, the impurity concentration distribution should actually be non-uniform due to the impurity compensation. This phenomenon is more obvious in a PPD structure due to the introduction of the deeply N-type implantation, which has been proved recently in our research.[10] We have been pursuing a more accurate model to provide actual designing guidance.

In this work, an analytical model for predicting the QE in a PPD structure is developed by taking account of the influence of the non-uniform doping N-type region in an actual process flow. Starting from approximating the upper and lower boundary junctions of the N-type region as the characteristics of abrupt and slow variations, respectively, the accurate junction model required for the QE modeling is obtained. With the solutions of the minority carrier steady-state diffusion equations and the barrier region photocurrent density equations, the QE analytical model is developed. The validity and accuracy of the proposed model are verified by a 160×160 pixels array.

2. Theory and modeling

2.1. Photo charge collection mechanism in a PPD

To model the QE in a PPD structure with three layers, the collection mechanism of photo-generated charges is first stud-

*Project supported by the National Defense Pre-Research Foundation of China (Grant No. 51311050301095).

†Corresponding author. E-mail: intercaochen@163.com

© 2014 Chinese Physical Society and IOP Publishing Ltd

ied. The typical schematic diagram of a 4T pixel is shown in Fig. 1(a), which consists of a PPD, a transfer gate (M1), a reset transistor (M2), an in-pixel amplifier (M3), and a selected switch (M4). The excited electrons originating in the PPD will transfer to the floating diffusion (FD) node and be converted into a voltage signal which can be output by a readout bus connected to the subsequent processing circuits.

The sectional view of the PPD is shown in Fig. 1(b) with the illustration of the corresponding photo charge collection mechanism. Conventionally, a completely PPD reset to a full depletion state is preferred to achieve empty well before exposure, pinning the potential of the buried N-type to the pinch-off voltage.[10] In this case, the depleted barrier regions formed by the upper and lower boundary junctions of the N-type are merged. When the PPD is illuminated by a light source with an intensity of Φ_{i0} at the top surface, the incoming photons can be absorbed and free electrons if their energies equal or exceed the band gap of silicon. The attenuation of the intensity is defined by the absorption coefficient α (in units of cm^{-1}) expressed as the following empirical equation:[11]

$$\alpha = \left(\frac{84.732}{\lambda} - 76.417\right)^2, \tag{1}$$

where λ represents the incident wavelength. So the absorption coefficient is a strongly decreasing function of wavelength.

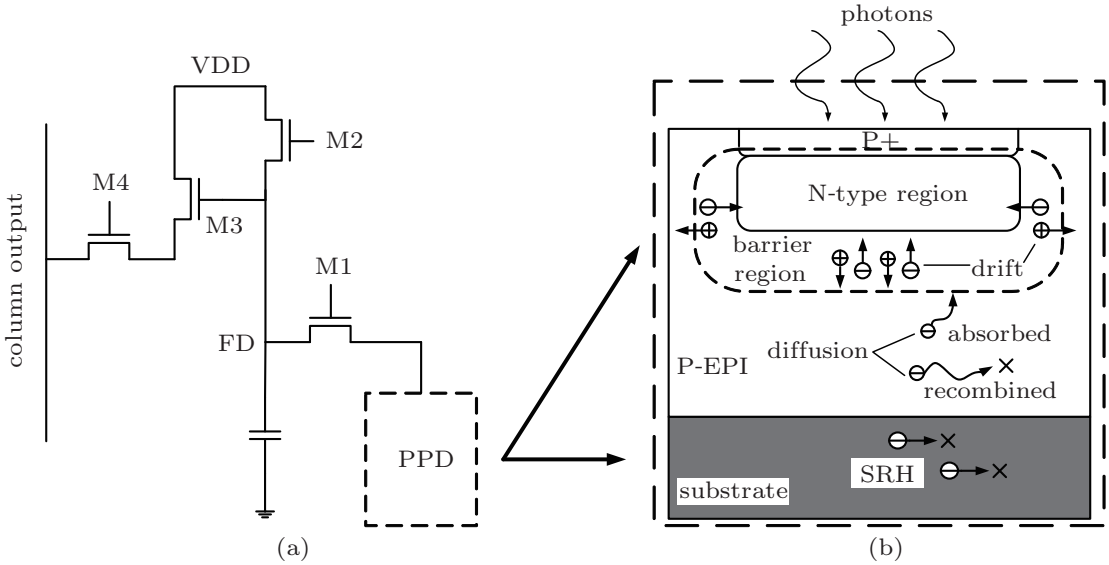


Fig. 1. Illustration of 4T pixel with a PPD structure. (a) 4T pixel circuit schematic plot; (b) photo charge collection mechanism in the PPD.

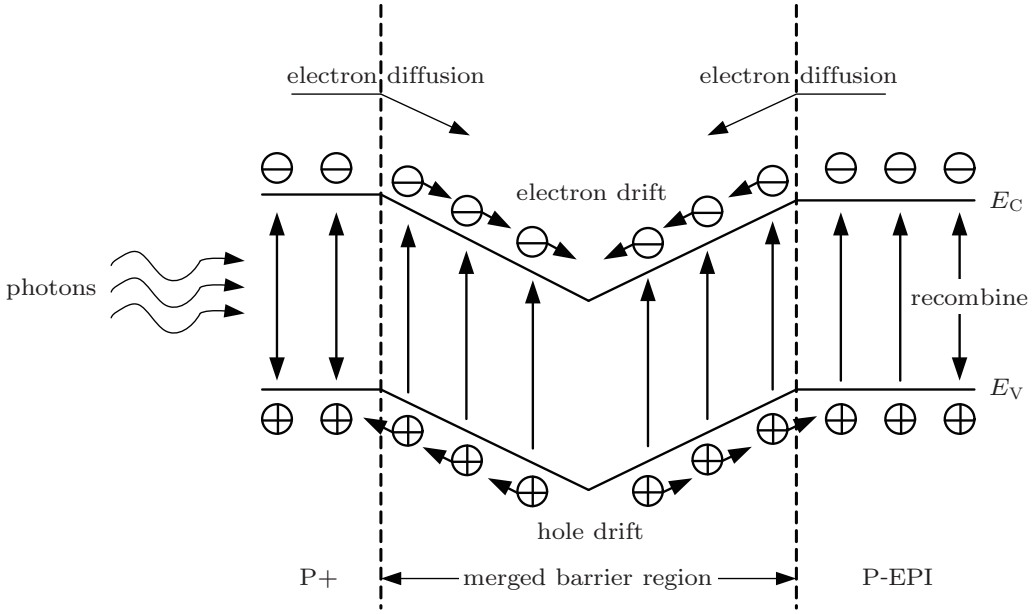


Fig. 2. Energy band diagram of a PPD in collection of photo charges.

The light intensity at a certain distance x from silicon top surface is expressed as

$$\Phi_{\mathrm{i}}(x) = \Phi_{\mathrm{i}0} \cdot \exp(-\alpha x), \tag{2}$$

therefore, the absorption depth α^{-1}, defined as the distance at which the light intensity decays to e^{-1} times of the initial value, increases with wavelength increasing. So, the electrons excited by short or medium wavelength illumination may drop into the merged barrier region, and be immediately collected as the photocurrent response according to the drifting force formed by the electric field. Of course, some electrons excited by ultra-short wavelength may be quickly recombined due to the high majority carrier density in surface P+ region, which cannot contribute to the responsivity, while the electrons excited by long wavelength illumination may drop deep into the epitaxial (EPI) layer or high doping substrate. As shown in Fig. 1(b), the non-equilibrium electrons in substrate are recombined mainly by Shockley–Read–Hall (SRH) mechanism due to the energy levels within the band gap created by defects,[12] while the others in the EPI layer beneath the barrier region mainly behave as diffuse movement in terms of the diffusion theory, part of them can reach the edge of the barrier region before recombination and be collected as the photocurrent response. The energy band diagram of a PPD in collection of photo charges is shown in Fig. 2, and the mechanism is clearly illustrated.

2.2. Junction model in the N-type region

It is derived from Eq. (1) that the absorption depth α^{-1} of the visible spectra (from 300 nm to 700 nm) varies between 0.01 μm and 5 μm, which means that the width of the N-type region has to be extended in a PPD structure for effective visible light responding in the merged barrier region established by the two boundary PN junctions. The extension leads to an obvious phenomenon of doping non-uniformly introduced by impurity compensation in the fabricating process of the N-type region. In this case, the upper junction for short wavelength absorption and the lower junction for long wavelength absorption located at the boundaries of the N-type region should present different characteristics, respectively. Therefore, during the modeling of the QE, the impurity concentration distribution may not be treated as uniform everywhere in the deeply extended N-type as specified in most of the references, and the junction characteristics should be prominent.

A simplified three-layer PPD configuration is shown in Fig. 3, which can be electrically divided into three districts, i.e., the P+ neutral region, the P-EPI neutral region, and the merged barrier region. As analyzed previously, the surface P+ implant should achieve high doping level as shallow as possible in order to achieve good blue responsivity and low dark current. So the upper junction between the surface P+ and N-type region can be equivalent to an abrupt junction.

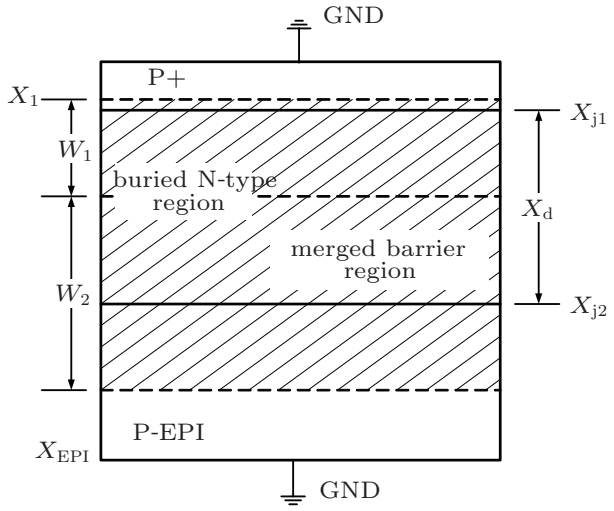


Fig. 3. A simplified three-layer PPD configuration.

By solving the Poisson's equation in the barrier region with the boundary conditions, the vertical width of the upper junction barrier region which is reversely biased by the pinch-off voltage V_{pinned} can be obtained as[13]

$$W_1 = \sqrt{(V_{\mathrm{bi1}} + V_{\mathrm{pinned}}) \left(\frac{2\varepsilon_{\mathrm{r}}\varepsilon_0}{q}\right) \left(\frac{N_{\mathrm{P+}} + N_{\mathrm{N}}}{N_{\mathrm{P+}} N_{\mathrm{N}}}\right)}, \tag{3}$$

where $N_{\mathrm{P+}}$ and N_{N} are the impurity concentrations of acceptors and donors, respectively, N_{N} can be regarded as the peak doping concentration in the N-type region; $\varepsilon_{\mathrm{r}}\varepsilon_0$ is the dielectric constant of silicon; q is the unit charge; V_{bi1} represents the built-in voltage in an equilibrium state and is given as

$$V_{\mathrm{bi1}} = \frac{k_0 T}{q} \left(\ln \frac{N_{\mathrm{N}} N_{\mathrm{P+}}}{n_{\mathrm{i}}^2}\right), \tag{4}$$

where k_0 is the Boltzmann constant, T is the temperature (the modeling is based on room temperature, 300 K), and n_{i} is the concentration of intrinsic carriers at 300 K.

Generally, $N_{\mathrm{P+}}$ is two orders of magnitude higher than N_{N},[14] so equation (3) can be written as

$$W_1 = \sqrt{\frac{2\varepsilon_{\mathrm{r}}\varepsilon_0}{qN_{\mathrm{N}}} (V_{\mathrm{bi1}} + V_{\mathrm{pinned}})}. \tag{5}$$

The distribution of impurities in the deep N-type region is determined by the impurity compensation between the N-type implant and EPI layer, so the doping concentration of the lower junction between the N-type and EPI slowly varies with a gradient factor σ_{j}. By solving the Poisson's equation in the barrier region with the boundary conditions, the vertical width of the lower junction barrier region which is reversely biased by the pinch-off voltage V_{pinned} can be obtained as[10]

$$W_2 = \sqrt[3]{\frac{12\varepsilon_{\mathrm{r}}\varepsilon_0 (V_{\mathrm{bi2}} + V_{\mathrm{pinned}})}{q\sigma_{\mathrm{j}}}}, \tag{6}$$

which is similar to Eq. (4):

$$V_{\rm bi2} = \frac{k_0 T}{q}\left(\ln\frac{N_{\rm Dmin}N_{\rm P-EPI}}{n_{\rm i}^2}\right), \tag{7}$$

where $N_{\rm Dmin}$ and $N_{\rm P-EPI}$ respectively represent the impurity concentrations of donors and acceptors in the infinitely small region around the metallurgical junction. In terms of the characteristic of the doping slowly varying junction, $N_{\rm Dmin}$ can be simply equal to $N_{\rm P-EPI}$ of the absolute value.

We have recently developed the pinch-off voltage model from the following equation[10]

$$\begin{aligned} X_{\rm d} = & \left[\sqrt{\frac{2\varepsilon_{\rm r}\varepsilon_0}{qN_{\rm N}}} - \beta\left(\frac{L_0 - L}{L_0}\right)^n\right]\cdot A \\ & + \frac{1}{2}\left[\sqrt[3]{\frac{12\varepsilon_{\rm r}\varepsilon_0}{q\sigma_{\rm j}}} - \beta\left(\frac{L_0 - L}{L_0}\right)^n\right]\cdot B, \end{aligned} \tag{8}$$

where

$$A = \left[\frac{k_0 T}{q}\left(\ln\frac{N_{\rm N}N_{\rm P+}}{n_{\rm i}^2}\right) + V_{\rm pinned}\right],$$

$$B = \left[\frac{k_0 T}{q}\left(\ln\frac{N_{\rm P-EPI}^2}{n_{\rm i}^2}\right) + V_{\rm pinned}\right],$$

with $X_{\rm d}$ being the N-type width, L_0 and L representing the lateral lengths of the PPD with and without lateral electric field effect, respectively, β being a constant that can be tested experimentally, and n being the degree of the lateral electric field effect. Then we have

$$V_{\rm pinned} = f\left(N_{\rm N}, X_{\rm d}, \sigma_{\rm j}, C\right), \tag{9}$$

where C is a constant determined by the parameters of pixel structure and material, $\sigma_{\rm j}$ is the item which can reflect the attenuation slope of the non-uniform doping level in N-type region.

Substituting Eq. (9) into Eqs. (5) and (6), respectively, the vertical widths of the upper and lower boundary barrier regions of the N-type, W_1 and W_2, can be accurately obtained. They are useful for the following QE model derivation.

2.3. Derivation of the QE model

The quantum efficiency $\eta_{\rm QE}$ is defined as

$$\eta_{\rm QE} = \frac{\mu_{\rm e}}{\mu_{\rm ph}}\cdot 100\%, \tag{10}$$

where

$$\mu_{\rm e} = \frac{A\cdot J_{\rm ph}\cdot t_{\rm exp}}{q}$$

and

$$\mu_{\rm ph} = \Phi_{\rm i0}\cdot t_{\rm exp} = \frac{A\cdot E\cdot t_{\rm exp}}{h(c/\lambda)}$$

respectively represent the number of photo charges that contribute to the photocurrent and the number of photons penetrating into the semiconductor, with A being the photo-sensing area of a PPD and $J_{\rm ph}$ the photocurrent density; $t_{\rm exp}$ is the exposure time; E is the light intensity in units of W·cm^{-2}; h is the Planck constant; c is the velocity of the light in vacuum. Then equation (10) can be replaced by

$$\eta_{\rm QE} = \frac{J_{\rm ph}\cdot h(c/\lambda)}{qE}, \tag{11}$$

indicating that QE depends on the illumination intensity, the incident wavelength and the total photocurrent density in a PPD. So, $J_{\rm ph}$ is the primary item in modeling QE for a given illumination condition.

Based on the charge collection mechanism analyzed previously, the total photocurrent density is mainly composed of two portions, one is the diffuse portion produced by minority carrier diffuse movement in the P+ and EPI neutral regions, and the other is the drift portion produced by the electron–hole pair separation under the action of electrical field in the barrier region. The photocurrent density in each region is modeled as done in the following study on the assumption that thermal generation current (or dark current) is neglected and all the carriers in the barrier region or within a diffusion length away contribute to the photocurrent with no recombination.

2.3.1. Diffuse portion

According to the diffuse theory, the behaviors of one-dimensional minority carriers in P+ and P-EPI neutral regions are depicted by a unified steady-state diffusion equation as follows:

$$D_{\rm n}\frac{\partial^2 n_{\rm p}(x)}{\partial x^2} - \frac{n_{\rm p}(x) - n_{\rm p0}}{\tau_{\rm n}} + G(x) = 0, \tag{12}$$

where $D_{\rm n} = k_0 T\mu_{\rm n}/q$ is the electron diffuse coefficient with $\mu_{\rm n}$ being the electron mobility, $\tau_{\rm n}$ is the lifetime of minority electrons, $n_{\rm p}(x)$ and $n_{\rm p0}$ represent the electron densities under illumination and equilibrium respectively, $G(x)$ is the number of electron–hole pairs per volume per second generated by illuminating, and it is expressed as

$$G(x) = -\frac{\partial\Phi_{\rm i}(x)}{\partial x} = \alpha\Phi_{\rm i0}\cdot\exp(-\alpha x). \tag{13}$$

The general solution of Eq. (12) can be obtained as

$$\begin{aligned} n_{\rm p}(x) = & \ n_{\rm p0} + k_{\rm n}\exp(-\alpha x) + C_1\exp\left(-\frac{x}{L_{\rm n}}\right) \\ & + C_2\exp\left(\frac{x}{L_{\rm n}}\right), \end{aligned} \tag{14}$$

where $k_{\rm n} = \Phi_{\rm i0}\alpha\tau_{\rm n}/(1-\alpha^2 L_{\rm n}^2)$, $L_{\rm n} = \sqrt{\tau_{\rm n}D_{\rm n}}$ is the diffusion length of electron.

By taking account of the surface recombination at Si–SiO_2 interface, the boundary conditions in P+ neutral region can be written as

$$\begin{cases} n_{\rm p}\left(X_{\rm j1}\right) = 0, \\ D_{\rm n}\left.\dfrac{\partial n_{\rm p}(x)}{\partial x}\right|_{x=0} = S_{\rm n}\left[n_{\rm p}(x) - n_{\rm p0}\right]\big|_{x=0}, \end{cases} \tag{15}$$

where S_n is the surface recombination velocity of electron.

The minority electrons in high doping substrate can hardly make contributions to the photocurrent, and the thickness of the EPI layer can be regarded as infinite ($X_{EPI} = \infty$). This important simplification is checked to be valid subsequently by device simulation data. So the boundary conditions in P-EPI neutral region is written as

$$\begin{cases} n_p\left(X_{j1}+W_1+W_2\right) = 0, \\ n_p\left(x\right)\big|_{x=\infty} = n_{p0}. \end{cases} \tag{16}$$

Subjecting Eqs. (15) and (16) to Eq. (14), the undetermined coefficients C_1 (C_1') and C_2 (C_2') can be obtained for both regions. The diffusion portion of the total photocurrent density in a PPD can be written as

$$J_{ph(diff)} = J_{P+} + J_{EPI} = \left| -qD_n \frac{\partial n_{p_P+}(x)}{\partial x}\bigg|_{x=X_{j1}} \right| + \left| -qD_n \frac{\partial n_{p_EPI}(x)}{\partial x}\bigg|_{x=X_{j1}+W_1+W_2} \right|. \tag{17}$$

2.3.2. Drift portion

The drift mechanism occurs in the merged barrier region. The photocurrent can be vertically divided into two parts according to the electrical field direction as shown in Fig. 3: one is in the direction from $X_{j1}+W_1$ to X_{j1}, the other is in the direction from $X_{j1}+W_1$ to $X_{j1}+W_1+W_2$. Doing so, the drift photocurrent density can be depicted as

$$J_{ph(dr)} = \left| -q\int_{X_{j1}}^{X_{j1}+W_1} G(x)\,dx \right| + \left| -q\int_{X_{j1}+W_1}^{X_{j1}+W_1+W_2} G(x)\,dx \right|. \tag{18}$$

Substituting Eq. (13) into Eq. (18), we have

$$J_{ph(dr)} = q\Phi_{i0}\left[2\exp\left(-\alpha X_{j1}-\alpha W_1\right) - \exp\left(-\alpha X_{j1}\right) - \exp\left(-\alpha X_{j1}-\alpha W_1-\alpha W_2\right)\right]. \tag{19}$$

2.3.3. QE model

Ultimately, according to Eqs. (17) and (19), the total photocurrent density in a PPD can be derived as

$$\begin{aligned} J_{ph} = J_{ph(diff)} + J_{ph(dr)} = {} & q\left(\alpha D_n k_n - \Phi_{i0}\right)\left[\exp\left(-\alpha X_{j1}\right) + \exp\left(-\alpha X_{j1}-\alpha W_1-\alpha W_2\right)\right] \\ & + \frac{qD_n}{L_n}\left[C_1\exp\left(-\frac{X_{j1}}{L_n}\right) - C_2\exp\left(\frac{X_{j1}}{L_n}\right) + C_1'\exp\left(-\frac{X_{j1}+W_1+W_2}{L_n}\right) - C_2'\exp\left(\frac{X_{j1}+W_1+W_2}{L_n}\right)\right] \\ & + 2q\Phi_{i0}\exp\left(-\alpha X_{j1}-\alpha W_1\right), \end{aligned} \tag{20}$$

where the significant items W_1 and W_2 have been modeled previously by taking account of the non-uniform doping distribution in the N-type region. Then substituting Eq. (20) into Eq. (11), we have

$$\eta_{QE} = f(W_1, W_2, \lambda, C') = f(N_N, X_d, \sigma_j, \lambda, C'), \tag{21}$$

where C' is a constant determined by the parameters of the pixel structure, wafer materials, and the steady light source. Therefore, equation (21) indicates that QE is determined by the fabricating process parameters of N-type and the incident wavelength for a certain PPD pixel. Figure 4 presents an actual process-like PPD doping profile combining with a transfer gate which is created by using Synopsys TCAD tools, and the meanings of the major parameters used for the proposed modeling are clearly marked and illustrated.

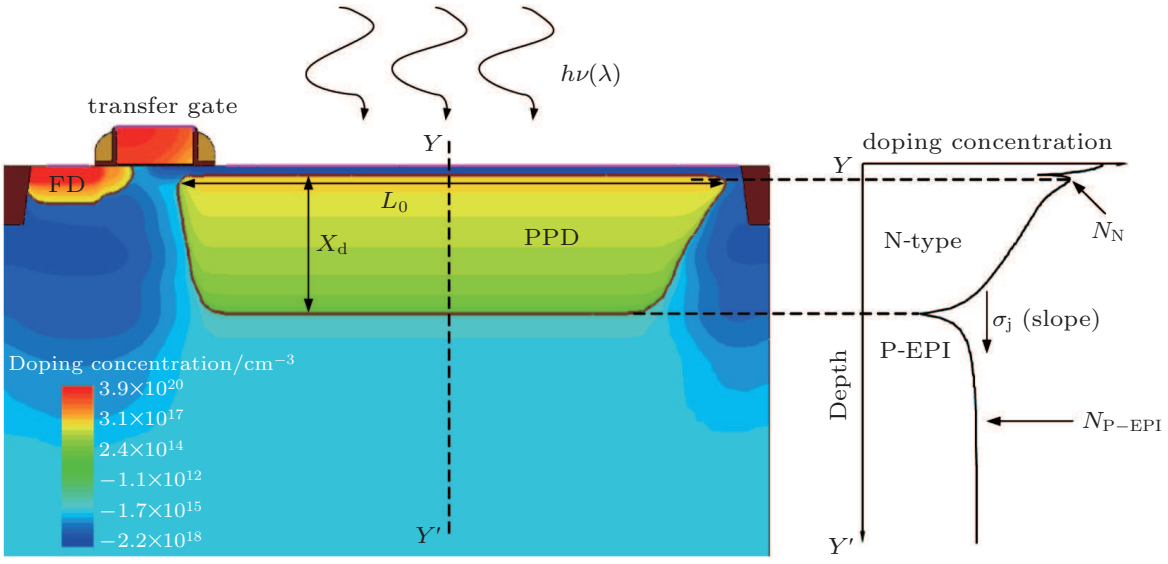


Fig. 4. (color online) An actual process-like PPD doping profile simulated by using Synopsys TCAD tools with illustrating of the proposed model parameters.

In summary, the proposed modeling can be simply divided into three steps: (i) derive the pinch-off voltage based on N-type process parameters; (ii) derive the vertical widths of the N-type upper and lower junction barrier regions based on the derived pinch-off voltage; (iii) derive the total photocurrent and QE based on the derived widths of the barrier regions.

3. Verification and discussion

3.1. Test setup

To demonstrate the validity and accuracy of the derived model, a prototype test chip of 160×160 pixel array is fabricated by deep sub-micrometer (DSM) 1P4M CIS dedicated technology, the pixel pitch is 6.6 μm with the fill factor of 57%. The overall layout of the chip is shown in Fig. 5.

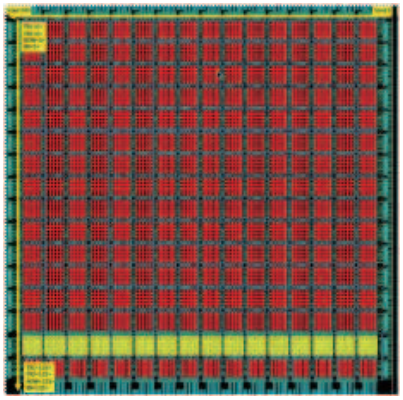


Fig. 5. (color online) Overall layout of the test chip of 160×160 pixels array.

The 10-μm EPI layer with a concentration of 10^{15} cm^{-3} is grown on a high doping (10^{18} cm^{-3}) substrate. The surface P+ region of the PPD is fabricated by implanting a dose of 2×10^{13} cm^{-2}. The N-type region of the PPD is fabricated by implanting various doses and energies which are listed in Table 1. The parameters N_N and σ_j which required for the modeling are extracted out by *C–V* measurements.[15] The parameter X_d can be measured by using the method of chemical reagent development which can distinguish between the P-type region and N-type region simply on the cross section of the cutting test chip.

Table 1. Summary of various N-type implant conditions and extracted parameters.

Dose/cm^{-2}	Energy/keV	N_N/cm^{-3}	X_d/μm	σ_j/cm^{-4}
5×10^{12}	50	1.30×10^{17}	0.4	1.28×10^{22}
	100	2.77×10^{17}	0.7	6.28×10^{21}
	150	2.83×10^{17}	1.0	4.29×10^{20}
	200	2.70×10^{17}	1.3	2.54×10^{20}
	250	1.96×10^{17}	1.5	1.14×10^{20}
3×10^{12}	150	1.27×10^{16}	0.9	5.93×10^{20}
4×10^{12}		2.01×10^{17}	0.9	4.72×10^{20}
5×10^{12}		2.83×10^{17}	1.0	4.29×10^{20}
6×10^{12}		3.56×10^{17}	1.0	3.93×10^{20}
7×10^{12}		4.38×10^{17}	1.0	2.87×10^{20}

The test pattern for the QE measurement is briefly shown in Fig. 6. Uniform monochromatic source illumination expected with an optional visible light wavelength can be generated by using an integrating sphere combined with a filter. Note that the light power monitor, which can measure the incident number of photons (μ_{ph}), is set at the external top surface of the chip. For doing so, η_{QE} can be directly measured as the external QE. When the incident photons penetrate into the upper layers of the semiconductor, the number of the photons decays to μ'_{ph} according to the transmission coefficient due to the reflection at the interface between each material (the optical absorptions within each material are ignored[16]). For the given technology, the used upper layer combination is Air/Si_3N_4/SiO_2/Si, so the total transmission coefficient T_{total} can be obtained from the refractive indexes of all materials above and given below.

$$T_{total} = \left[1-\left(\frac{n_{air}-n_{Si_3N_4}}{n_{air}+n_{Si_3N_4}}\right)^2\right]\cdot\left[1-\left(\frac{n_{Si_3N_4}-n_{SiO_2}}{n_{Si_3N_4}+n_{SiO_2}}\right)^2\right] \times\left[1-\left(\frac{n_{SiO_2}-n_{Si}}{n_{SiO_2}+n_{Si}}\right)^2\right]. \tag{22}$$

Then, the actual internal QE modeled in previous section can be extracted out as

$$\eta'_{QE} = \frac{1}{T_{total}}\cdot\eta_{QE}. \tag{23}$$

The number of the generated electrons μ_e is extracted out by the photocurrent measurements within a certain exposure time.

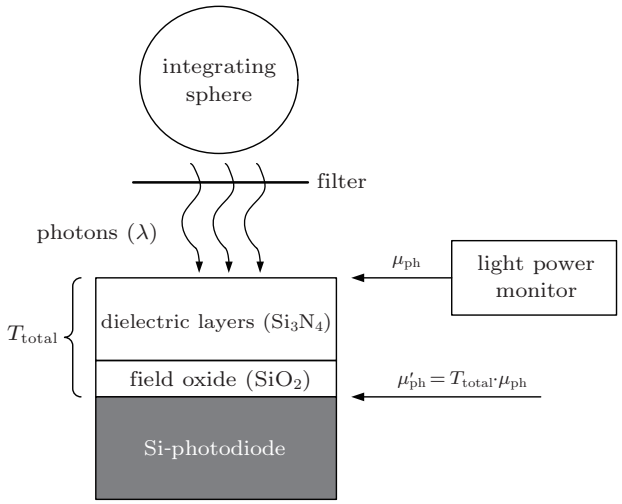


Fig. 6. Brief illustration of light power test pattern for QE measurement.

For calculating the proposed model, the typical values of the parameters are used (according to the appearing orders in this paper): $\varepsilon_r\varepsilon_0 = 1.05\times10^{-12}$ F·m^{-1}, $q = 1.6\times10^{-19}$ C, $k_0T = 0.026$ eV, $n_i = 1.5\times10^{10}$ cm^{-3}, $\beta = 1.3$, $n = 1.5$,[10] $h = 6.63\times10^{-34}$ J·s, $c = 3\times10^8$ m·s^{-1}, $\mu_n = 1.45\times10^3$ cm^2·V^{-1}·s^{-1}, $\tau_n = 2\times10^{-4}$ s, and $S_n = 4\times10^2$ m·s^{-1}.

3.2. Results and discussion

The feasibility of the important simplification of the infinite thickness EPI layer during the QE modeling is first checked by using finite difference time domain (FDTD)[17] device simulation based on the PPD model presented in Fig. 4. The incident wavelength is set to be 700 nm for a furthest photo electrons diffusion in the EPI layer. The sectional view of the FDTD light intensity attenuation in the silicon with an incident intensity of 0.05 W·cm^{-2} is presented in Fig. 7(a), and the corresponding photo electron density distribution during the stable illumination is shown in Fig. 7(b). It is extracted that the electron densities at the depths of 5 μm and 10 μm (the positions which respectively represent the light absorption distance and the EPI edge) are 1.34×10^{11} cm^{-3} and 1.09×10^{9} cm^{-3}, respectively. The latter one shows two orders of magnitude smaller than the former, indicating that the non-equilibrium electrons excited by the wavelength of 700 nm nearly disappear at the EPI edge due to diffusion and recombination, so do the electrons excited by other visible light

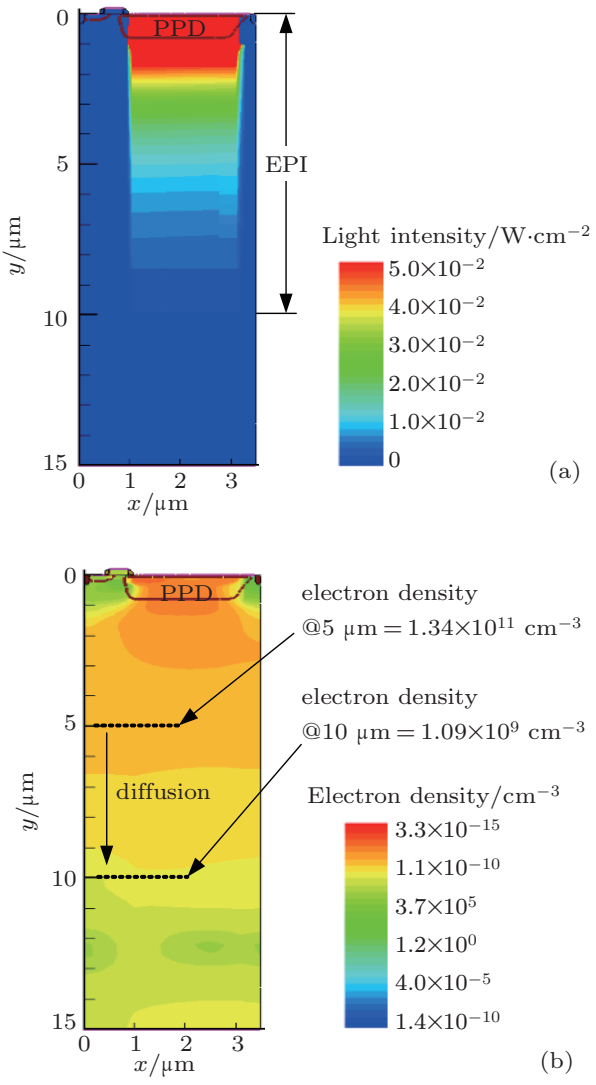


Fig. 7. (color online) Sectional view of the PPD simulated by using FDTD method with an incident wavelength of 700 nm. (a) Distribution of the light intensity; (b) distribution of the photoelectron density.

wavelengths with shorter absorption distances. Therefore, the 10-μm EPI layer can be regarded as infinitely thick, and supports our theoretical results.

Figure 8 shows the QEs calculated from the proposed model, which are compared with the measurement results for different N-type implantation energies within an identical dose of 5×10^{12} cm^{-2}. The model predictions are in excellent agreement with the measurements at the incident wavelengths of 500 nm (green) and 700 nm (red). The QE is much higher at the green wavelength, because the absorption depth is comparable to the depth of the depleted barrier region established by the lower junction of the N-type, causing most of the excited electrons to drift as the photocurrent response. When N-type implantation achieves a specific energy of 150 keV, the depletion depth exceeds the green light absorption depth, so as the implant energy increases, the number of drifted electrons is nearly fixed thus stabilizing the QE (the number of diffused electrons from EPI layer is so small that it can be ignored compared with the drifting ones). The QE at the red wavelength presents a linear growth with the N-type implantation energy increasing because the intensity of the red wavelength can be approximately regarded as uniform along the transmission path without attenuation due to the low value of the absorption coefficient according to Eq. (1). Therefore, the number of drifting electrons increases uniformly as depletion depth increases.

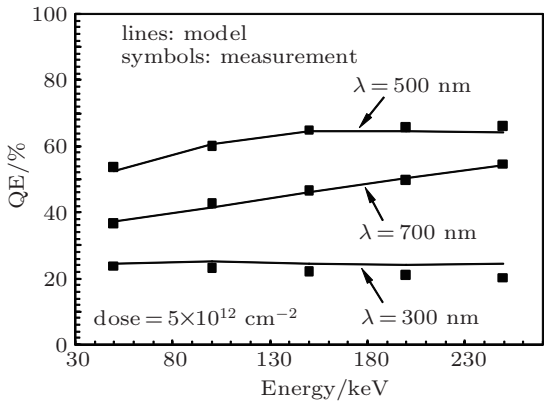


Fig. 8. Comparisons of the QE between the model predictions and the measurement results under various N-type implant energies.

However, the model predictions at a wavelength of 300 nm (blue) shows slightly deviation from the measurements. The observed slow decrease of the measurements can be explained by the fact that as the N-type implantation energy increases, the peak position of the donor impurity doping level that presents the known vertical Gaussian distribution enters deeper into the silicon, thus deepening the upper junction of the N-type region which is neglected in the proposed model. Hence, part of the electrons excited by blue wavelength near the surface are hardly being collected by the barrier region, thereby causing a worse blue response. The high doping level of the surface P+ makes the junction deepen imperceptibly,

which can be verified by using TCAD process simulations as shown in Fig. 9.

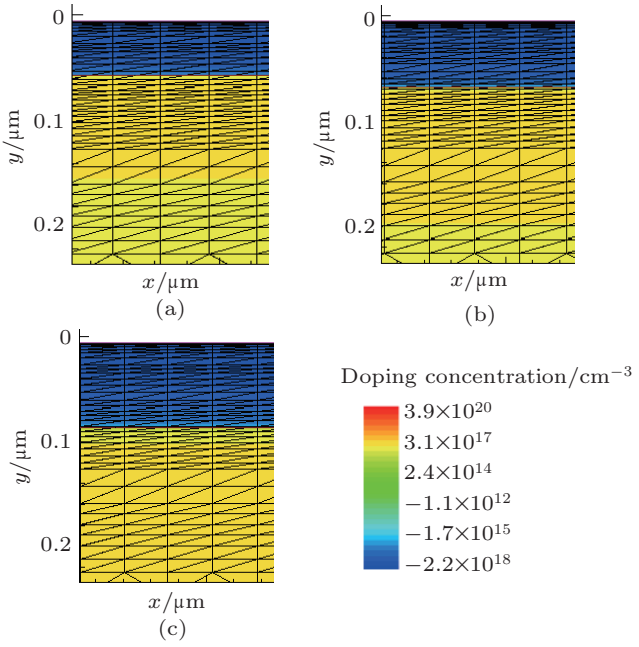


Fig. 9. (color online) Simulation results at energies of (a) 50 keV, (b) 150 keV, and (c) 250 keV, showing that the N-type upper junction deepens with the implant energy increasing.

Figure 10 shows the predictions from the proposed model, which are compared with the measurement results for different N-type implant doses at an identical energy of 150 keV. Similarly, the results from the proposed model show good agreement with the measurements under green and red wavelength illumination. The QE shows insensitive with the N-type implant dose increasing because the value of implant dose mainly dominates the peak doping level in N-type region near the upper junction, and can hardly affect the drift–diffuse behavior of the electrons excited by green and red wavelengths.

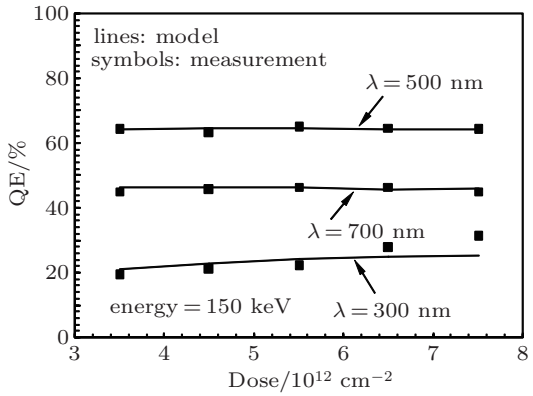


Fig. 10. Comparisons of the QE between the model predictions and the measurement results under various N-type implant doses.

The observed slow increase of the measurements under blue wavelength illumination can be explained by the fact that as the peak doping level of the N-type increases with the implant dose growth, the N-type region extends into the surface P+ region due to the impurity compensation, causing the upper junction of the N-type to enter into the silicon more shallowly with a better blue wavelength response which is verified by using TCAD process tool as shown in Fig. 11.

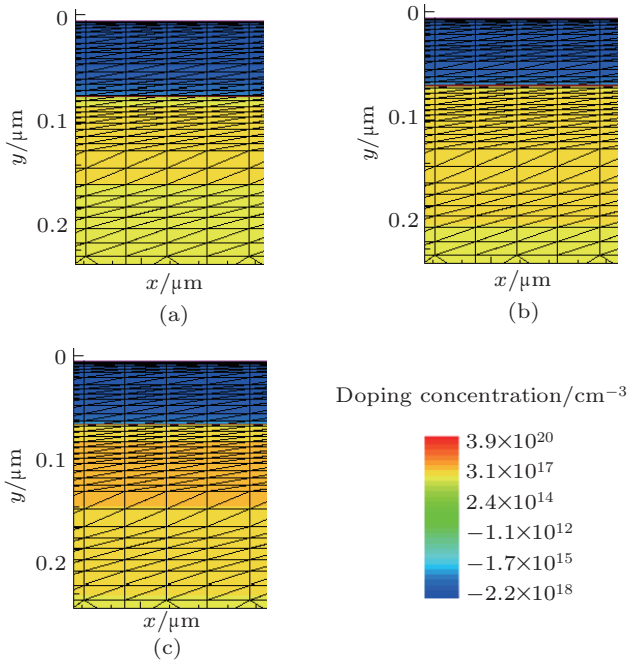


Fig. 11. (color online) Simulation results at doses of (a) 3×10^{12} cm^{-2}, (b) 5×10^{12} cm^{-2}, and (c) 7×10^{12} cm^{-2}, showing that the N-type upper junction shallows with the implant dose increasing.

Figure 12 shows the measurement results under full visible spectra compared with the predictions of the models by taking account of non-uniform (proposed) and uniform (traditional) doping distribution N-type respectively. Note that the proposed model shows a good agreement with the measurements under the given N-type implantation energies. By comparing Fig. 12(b) with Fig. 12(a), a dramatically positive deviation of traditional model predictions from the measurements is observed as implantation energy increases from 50 keV to 150 keV, especially at medium or long incident wavelength. The reason can be explained as the fact that owing to the absence of the gradient attenuation doping of the N-type region in the traditional model, a stronger pinch-off voltage must be supplied to exhaust the whole unified doping neutral region from top position to bottom, causing a volume enlargement of the merged barrier region especially the lower one for responding to the major medium or long wavelength. The extension of the N-type width which is induced by the implantation energy growth leads to a more obvious phenomenon of doping non-uniformly, causing the dramatic deviation of the traditional model observed in the figure. Therefore, the proposed model is proved to be more accurate in featuring the variations of the QE versus actual process changes.

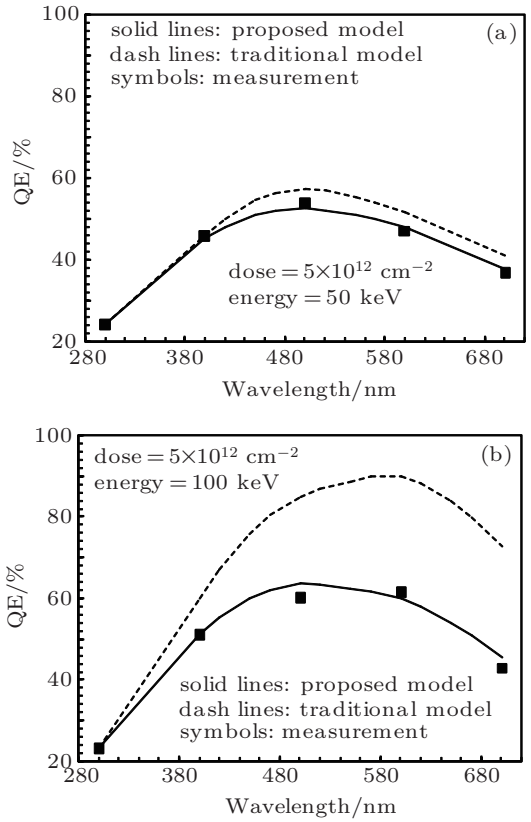


Fig. 12. Comparisons of measurement result between the proposed and the traditional model under different N-type implant energies of (a) 50 keV and (b) 100 keV.

4. Conclusions

An analytical model for predicting the QE of CMOS image pixels with three-layer PPD structure is developed. The model takes account of the different PN junction characteristics at the upper and lower boundaries of the photo-sensing N-type region, which actually exists in a process flow. Verification with the test chip measurements under various N-type implantation conditions proves the accuracy of the model under typical green and red wavelength illumination. The mechanism of a slight deviation of the model from the measurements at blue wavelength is analyzed. Comparison between the proposed model and the traditional uniform N-type doping model proves that the proposed model presents more practical theoretical guidance in fabricating process for the QE design.

References

[1] Shoushun C, Boussaid F and Bermak A 2008 *IEEE Sensors Journal* **8** 286
[2] Chen S, Tang W and Culurciello E 2010 *Proceedings of* 2010 *IEEE International Symposium on Circuits and Systems (ISCAS)*, May 30–June 2, 2010, Paris, France, p. 1404
[3] He J, Su Y M, Ma Y T, Chen Q, Wang R N, Ye Y, Ma Y and Liang H L 2012 *Chin. Phys. B* **21** 076104
[4] Goiffon V, Virmontois C, Magnan P, Cervantes P, Place S, Gaillardin M, Girard S, Paillet P, Estribeau M and Martin P 2012 *IEEE Trans. Nucl. Sci.* **59** 918
[5] Raverzzi L, Betta G F, Stoppa D and Simoni A 2000 *Microelectronics Journal* **31** 227
[6] Desai N R, Hoang K V and Sonek G J 1993 *IEEE Trans. Education* **36** 357
[7] Perry R J and Arora K 1996 *Proceedings of IEEE Southeastcon Bringing Together Education Science and Technology*, April 11–14, 1996, Tampa, USA, p. 374
[8] Djite I, Estribeau M, Magnan P, Rolland G, Petit S and Saint-Pe O 2012 *IEEE Trans. Electron. Dev.* **59** 729
[9] Zeng H M, Wei T C and Zheng R 2011 *IEEE International Conference on Signal Processing, Communications and Computing (ICSPCC)*, September 14–16, 2011, Xi'an, China, p. 1
[10] Cao C, Zhang B, Wu L S, Li X and Wang J F 2014 *Chin. J. Semicond.* **35** 074012
[11] Liu W J, Chen O T, Dai L K and Weng P K 2001 *Proceedings of the* 5*th IEEE International Workshop on Behavioral Modeling and Simulation*, October 10–12, 2001, Santa Rosa, USA, p. 102
[12] Puliyankot V and Hueting R J 2012 *IEEE Trans. Electron. Dev.* **59** 26
[13] Liu E K, Zhu B S and Luo J S 2012 *The Physics of Semiconductors* (Beijing: Electronics Industry) p. 177 (in Chinese)
[14] Lee P P 2000 U.S. Patent 5 625 210 [2000-08-08]
[15] Liu E K, Zhu B S and Luo J S 2012 *The Physics of Semiconductors* (Beijing: Electronics Industry) p. 181 (in Chinese)
[16] Ni J H 2008 "CMOS Image Sensors Sensitivity Improvement via Process Optimization" (MS Thesis) (Shanghai: Shanghai Jiao Tong University) (in Chinese)
[17] Wu K, Wei T B, Lan D, Zheng H Y, Wang J X, Luo Y and Li J M 2014 *Chin. Phys. B* **23** 028504